Experimental Thermal and Fluid Science 148 (2023) 110981

Contents lists available at ScienceDirect

Experimental Thermal and Fluid Science

journal homepage: www.elsevier.com/locate/etfs

Twin background subtraction technique: A novel infrared technique for simultaneous thickness and temperature measurements of micro films

R. Clavenna *, L. Araneo

Politecnico di Milano, Energy Department, Italy

ARTICLE INFO

Keywords:
Liquid film thickness
Liquid film temperature
Micro film
Infrared measurement
Microchannel

ABSTRACT

The study proposes a novel non-intrusive infrared technique to measure simultaneously the thickness and temperature of a thin layer that is semi-transparent to infrared radiation. The measurement method has been called Twin Background Subtraction technique. The technique simultaneously exploits the mid-wave IR emission from the film to be measured and the radiation attenuation by the same film of the emission coming from two backgrounds at different constant temperatures. This study discusses the method theoretically and experimentally, focusing on the uncertainties and the dependence on different parameters of the set-up and fluid physical properties.

The fluid adopted for the film is water, and various tests have been carried out by changing its temperature between 15 and 50 °C and its thickness from 0 to 500 μm. The TBS technique was proven to be of interest for studying micro to mini films both from a qualitative and quantitative point of view for water films ranging between 10 μm and 350 μm.

1. Intro

In literature, there are several different experimental studies proposed to directly measure the temperature of a liquid by the use of intrusive instruments, e.g. thermocouples, and non-intrusive, e.g. direct infrared measurement, when the liquid is sufficiently thick that its transmissivity is sufficiently low to be neglected and the liquid can be approximated to an opaque body. Meanwhile, the liquid film thickness can be measured with various techniques developed specifically for their field of application depending on the range of thickness, fluid properties, wall material and gas presence. In the work of Tibiriçá et al. [1], there is a comprehensive list of possible techniques for thickness measurements applied to micro-scale and two-phase flow systems. The variety of techniques found in literature adopted for liquid film thickness measurement can be classified by different criteria, including dimensions, like point measurements, linear, whole field; and by the instrument or physical principle used like: laser, optic, ultrasonic and conductance techniques. Most of the laser techniques are based on monochromatic light absorption through the liquid or by induced fluorescence of the film volume to generate contrast at the gas–liquid interface. Mignot et al. [2] and Dupont et al. [3] simultaneously investigated film thickness up to 2 mm and film temperature in evaporating condensing environment with two different measurement methods: near-infrared light measuring method to investigate the film temperature and Mid-wave infrared thermography to study the film thickness, respectively inspecting a vessel FOV of approximately 153.6 mm × 192 mm at 1 m distance. The study focused on thermodynamic conditions encountered in containment during a severe accident scenario. Morokuma et al. [4] proposed a measurement method for the change in thickness of a liquid film formed between colliding bubbles based on combined laser extinction and a laser interferometric measurement system. Schmidt et al. [5] developed and validated an absorption-based laser sensor to investigate dynamically changing liquid film thicknesses. Han et al. [6], in their work, adopted Laser Focus displacement meter method to measure locally the film formed between the tube and the vapour bubble. They tested different pipe inner diameters from 0.3 to 1.3 mm with ethanol, water and FC-40, developing a model for the initial film thickness based on the capillary number, Reynolds number, and Weber number. Other laser techniques adopted Laser-Induced fluorescence to study the film thickness and analyse the flow behaviour in a gas–liquid flow [7,8]. The optical techniques applied by Riaño et al. [9] in their work is based on the acquisition of images of dispersed oil-in-water and annular flows with a high-speed video camera, and then by image processing techniques, the film thickness is quantified near the pipe wall. Similarly, Donniacuo et al. [10] proposed a method based on detecting

* Corresponding author.
E-mail address: riccardo.clavenna@polimi.it (R. Clavenna).

https://doi.org/10.1016/j.expthermflusci.2023.110981
Received 9 January 2023; Received in revised form 17 March 2023; Accepted 5 June 2023
Available online 8 June 2023

Nomenclature

0	Characteristic, reference
BG1, BG2	background 1 and 2
$\dot{E}$	Radiation power or energy
F	film
FOV	Field of View
ITTM	infrared temperature and thickness measurements
L	thickness, length [μm]
L_0	reference thickness, giving attenuation $\alpha = 1/\xi$
NUC	Non Uniformity Correction
ROI	Region of Interest
S	signal
S1,S2	Signal 1 and signal 2 of attenuated radiation of BG1 and BG2, respectively.
T	temperature
TBS	Twin Background Subtraction
u	uncertainty
W	wall
α	Absorptance
ε	emissivity
λ	wavelength
ξ	linear absorption coefficient
ξ_{100}	equivalent linear absorption coefficient measured with a film thickness $L_{film} = 100$ μm
ρ	reflectance
σ	Stefan-Boltzmann constant $= 5.67 \times 10^{-8}$ W m^{-2} K^{-4}
τ	transmittance

liquid–vapor and liquid–solid interfaces. For each flow condition, about 2000 frames per second were recorded with a high-speed camera and then processed to obtain the average liquid film measurement and the cross-section void fraction of a R245fa. Ultrasonic methods are based on interfacial reflection, Wang et al. [11] proposed an ultrasonic method named "Ultrasonic Echo Resonance Main Frequency" (UERMF), able to measure the liquid film thickness and overcome the limitations of common ultrasonic pulse-echo methods, which cannot measure thin films affected by noise end echoes. Yu et al. [12] studied an algorithm that simultaneously utilizes the amplitude and the phase of the complex ultrasonic reflection coefficient for a direct calculation instead of an iterative approximation to estimate a known oil film thickness. The conductance method is based on liquid and gas different conductivity values. Wang et al. [13] presented an analytical solution to estimate the liquid film thickness in a two-phase annular flow through a circular pipe using electrical resistance tomography. The liquid film thickness for an arbitrary annular flow was estimated by comparing the resistance values for concentric and eccentric annular flows. Tiwari et al. [14] presented an approach toward enhancing the measuring range of high-speed sensors for the measurement of liquid film thickness based on electrical conductance by measuring the current generated between a pair of electrodes. Choi et al [15] developed an electrical conductance sensor to measure the liquid film's local thickness in a downcomer annulus of a nuclear reactor pressure vessel, to investigate the behaviour of liquid films under emergency core cooling. In literature, just the work of 2021 by Wu et al. [16] developed a technique that simultaneously measures liquid film thickness and temperature. The study's method is based on local measurement with diode laser absorption spectroscopy (DLAS) and focused on film thickness over a metal plate in the range of 200–800 μm, the upper limit due to the absorption saturation. The film was studied in horizontal and tilted conditions. The average relative deviations of 3.3% film thicknesses and 2.0% film temperature are obtained by comparing the measurements of the DLAS technique to the measurement of the ultrasonic pulse-echo method (UPEM).

In this study, we aim to propose an alternative, less complex, innovative technique that is non-intrusive, with a wide measurement field and applicable to many sectors where the study of thin films is of particular interest. The technique is proposed and developed within the ESA project TOPDESS to characterize the liquid film around a vapour bubble formed in a pulsating heat pipe [17] during microgravity tests [18]. The technique is based on the attenuation of twin signals from two different emitting black bodies, called backgrounds, at different homogenous temperatures and passing through the studied film. Furthermore, based on a single mid-wave infrared camera, the field of view can be optimized for the study of interest from a higher spatial resolution to a broader field of view. In this study, we developed the TBS technique both theoretically and experimentally with a validation set-up and different calibrating thin films of water in the range of 0–500 μm and temperature between 15 and 50 °C.

2. Theory

The Twin Background Technique aims to measure the temperature and the thickness of a thin liquid layer with a single measuring

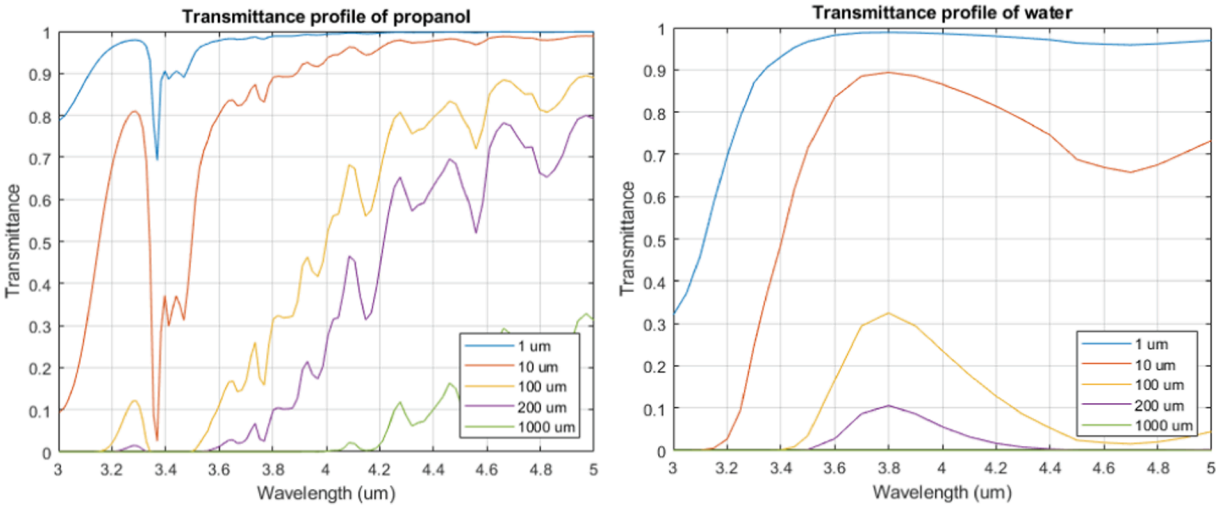

Fig. 1. Transmittance τ_λ of water and propanol in the 3–5 μm bandwidth and film thickness 1–1000 μm.

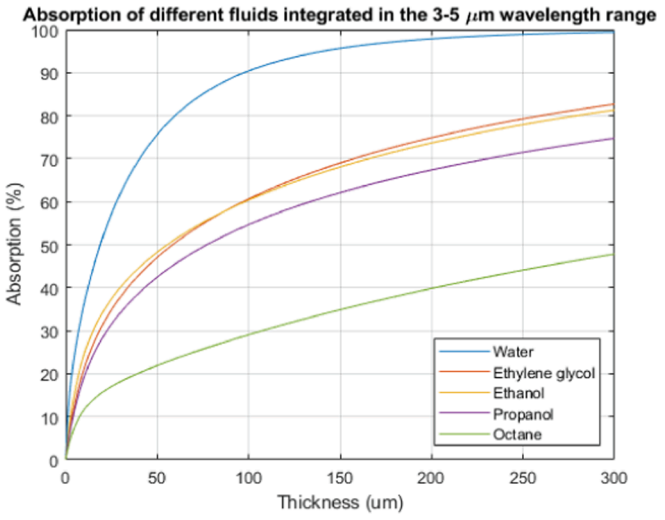

Fig. 2. Different radiation absorption profiles of different fluids.

instrument and an easy set-up. The use of the technique could be applied to many thermofluidic investigations like the biphase fluid motion investigations inside channels to measure the liquid film around bubbles, the condensation phenomena to measure the first formation of droplets or films on a surface and their accretion with the temperature gradient distribution, the evolution of a liquid film formed by a droplet impact and its evaporation, but also to industrial production monitoring processes involving the production and lamination of solid films.

The technique is developed using a mid-wave infrared thermal camera, but it is not limited to this device and, in principle, can be extended to other wavelengths and other measurement instruments.

In the infrared wavelength, the thin liquid film behaves as participating media that emits, scatters, transmits and reflects the radiation. The TBS technique is developed to work with a thin layer of liquid that behave as semi-transparent in the infrared wavelength investigated. Hence, the technique is practically limited to a subgroup of fluids.

Specifically, the liquid should have some properties that make it suitable for its use with the technique: reflectance is low or can be assumed as negligible for the application reducing the unwanted radiation reflection from the liquid container and environmental radiation if the environment is unchanging over time they can be compensated for by proper calibration, scattering is negligible avoiding reflections within the liquid, and photoluminescence is negligible eliminating problems related to emission in other wavelengths.

Different fluids will have different absorption spectra in the used wavelength range resulting in a different transmittance function of the liquid thickness. Therefore, starting from the extinction coefficient of the fluid k_F, defined the wavelength λ, its monochromatic linear absorption coefficient $\xi_{\lambda,F}$ is calculated:

$$\xi_{\lambda,F} = \frac{4\pi k_F}{\lambda} \tag{1}$$

Then, with the Lambert-Beer law, it is possible to estimate the transmittance for each wavelength through a flat sheet of the fluid of thickness, L_F:

$$\tau_{\lambda,F} = e^{-\xi_{\lambda,F} L_F} \tag{2}$$

Fig. 1 plots two examples of different fluid response functions in the same wavelength band with increasing thickness. Water and propanol transmittance profiles are vastly different, making propanol more "transparent" at a higher thickness than water that saturates toward zero around 300 μm. Hence depending on the application and on the chosen fluid, it is possible to estimate the theoretical thickness full scale of the applied TBS technique (see Fig. 2).

The TBS technique exploits the signal attenuation in the mid-wave IR from two backgrounds at different constant temperatures. The radiation passing through the semi-transparent medium decreases depending on the thickness of the layer. The thicker it is, the lower will be the transmitted radiation and the higher the emission of the fluid itself.

The general total radiation power Ė received by the camera [19] from an object can be expressed as:

$$\dot{E}_{tot} = \varepsilon\tau\dot{E}_{obj} + (1-\varepsilon)\tau\dot{E}_{amb} + \varepsilon\dot{E}_{atm} \tag{3}$$

The IR camera will receive a radiative heat flow interpreted as the equivalent temperature of an emitting body, which we will call T_S (temperature of the signal). The radiation is then expressed as the sum of the radiation from the background with its temperature T_{BG} and emissivity, attenuated by the layer, and the emission from the layer itself, giving the following expression:

$$\alpha_{\lambda,S}\sigma T_S^4 = \varepsilon_{\lambda,BG}\sigma T_{BG}^4 \bullet \tau(L_F)_{\lambda,F} + \varepsilon(L_F)_{\lambda,F}\sigma T_F^4 \tag{4}$$

By properly calibrating the thermal camera, the emissivity and absorptance coefficients are corrected, and the equivalent temperature of the signal can be further simplified if the solution to the problem does not depend on the incidence angle of the radiation.

$$T_{\lambda,F} = \left(\varepsilon_{\lambda,BG}T_{BG}^4 \bullet \tau_{\lambda,F} + \varepsilon_{\lambda,F}T_F^4\right)^{0.25} \tag{5}$$

The reflectance of the sapphire to the mid-wave IR is about 6.3% [20], and the normal reflectance at the interface between water and sapphire with normal radiation can be estimated by the Fresnel equation as 1.1%. Both terms are compensated with a proper calibration procedure and unchanging external conditions. In the experimental set-up, the film's thickness is increased by enlarging the top spacing between two sapphires forming a wedge shape. The maximum angle variation is about 0.6° resulting from being negligible in terms of sapphire reflectance (less than 0.1%). Thus the sapphire windows can be assumed semi-transparent to the infrared radiation:

$$\alpha_\lambda + \tau_\lambda = 1, \rho_\lambda = 0 \tag{6}$$

We can assume that all the bodies considered follow Kirchhoff's law and their response in the range of wavelength is equal to the response in the monochromatic wavelength:

$$\varepsilon = \alpha \tag{7}$$

Having experimentally determined that under steady conditions, the temperature of the sapphire walls enclosing the liquid can be assumed equal to the fluid temperature and that the emissivity and the transmissivity coefficients are equal to:

$$\tau_w = 1 - \alpha_w \tag{8}$$

The signal (Equation (4) depends on two unknowns, the film temperature T_F and the film thickness L_F. By switching as background a second black body at a different constant temperature, we can collect separately two different signals measurements. Hence, it is possible to solve the system of two unknowns with two equations. Assuming constant properties values in the wavelength investigated it is possible to add all the IR contributions directly participating in the two signals S_1, S_2 expressed as apparent temperatures T_{S1} and T_{S2}:

$$T_{S1} = \left(\varepsilon_{BG,1}T_{BG,1}^4\tau_A + \varepsilon_W T_W^4\tau_B + \varepsilon_F T_F^4\tau_C + \varepsilon_W T_W^4\tau_D + \varepsilon_{air}T_{air}^4\right)^{0.25} \tag{9}$$

$$T_{S2} = \left(\varepsilon_{BG,2}T_{BG,2}^4\tau_A + \varepsilon_W T_W^4\tau_B + \varepsilon_F T_F^4\tau_C + \varepsilon_W T_W^4\tau_D + \varepsilon_{air}T_{air}^4\right)^{0.25} \tag{10}$$

$$\tau_A = \tau_F\tau_w^2\tau_{air} \tag{11}$$

$$\tau_B = \tau_F\tau_w\tau_{air} \tag{12}$$

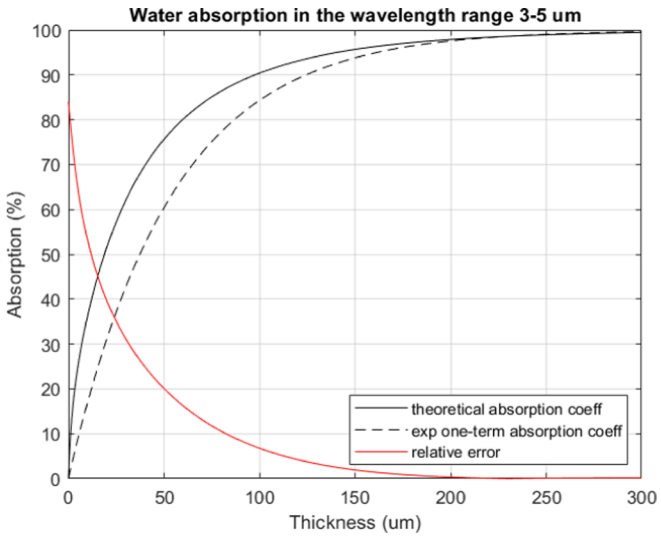

Fig. 3. Radiation absorption of water difference between the actual theoretical curve and the one-term exponential.

$$\tau_C = \tau_w \tau_{air} \tag{13}$$

$$\tau_D = \tau_{air} \tag{14}$$

Considering that in fluid visualization, we have a distance between the camera and the target in the range of meters at maximum to provide sufficient FOV resolution, it is possible to neglect the air influence; moreover, the temperature influence on the walls' transmissibility is limited, and in case of stationary systems in which the fluid is thermalized it is possible to assume its temperature equal to the temperature of the fluid. Accordingly, under the assumption that the walls containing the fluid are quasi-transparent bodies and follow the same Equation (6) with $\alpha_w \ll \tau_w$ the system of equations can be further simplified as follow:

$$T_{S1} = \left(\varepsilon_{BG,1} T_{BG,1}^4 \tau_A + \varepsilon_W T_W^4 \tau_B + \varepsilon_F T_F^4 \tau_C + \varepsilon_W T_W^4\right)^{0.25} \tag{15}$$

$$T_{S2} = \left(\varepsilon_{BG,2} T_{BG,2}^4 \tau_A + \varepsilon_W T_W^4 \tau_B + \varepsilon_F T_F^4 \tau_C + \varepsilon_W T_W^4\right)^{0.25} \tag{16}$$

$$\tau_A = \tau_F \tau_w^2 \tag{17}$$

$$\tau_B = \tau_F \tau_w \tag{18}$$

$$\tau_C = \tau_w \tag{19}$$

By choosing a background coating with an emissivity ε_{BG} close to 1, it is possible to calculate the transmissibility τ_F and the temperature T_F of the film as:

$$\tau_F = \frac{T_{S,1}^4 - T_{S,2}^4}{\tau_W{}^2 \left(\varepsilon_{BG1} T_{BG1}{}^4 - \varepsilon_{BG2} T_{BG2}{}^4\right)} \tag{20}$$

$$T_F = \left(\frac{\varepsilon_{BG1} T_{BG1}{}^4 T_{S2}^4 - \varepsilon_{BG2} T_{BG2}{}^4 T_{S1}^4}{T_{S,1}^4 - T_{S,2}^4 - \varepsilon_{BG1} T_{BG1}{}^4 + \varepsilon_{BG2} T_{BG2}{}^4}\right)^{1/4} \tag{21}$$

The monochromatic linear absorption coefficient ξ_λ of the investigated fluid can be estimated from spectroscopy databases from the refractive index [20] or the absorption cross-section [21]. By integrating Equation (2) in the measured wavelength range, we get the equivalent averaged IR transmissibility of the fluid, $\overline{\tau_F}$:

$$\overline{\tau_F} = \int_{\lambda_1}^{\lambda_2} e^{-L_F \xi_\lambda} d\lambda \tag{22}$$

The curve shape depends on the weight of the ξ_λ term with the wavelength, with a shape that could be expressed as a one-term exponential in the simplest case and as an n-term exponential, depending on the accuracy required. Different fluids will present different radiation absorption profiles. Hence the absorption profile of the fluids will differ with the fluid. For example, from a theoretical point of view, pure water will saturate at around 300 μm within the chosen wavelength range of 3–5 μm with a curve similar to a logarithmic curve. On the contrary octane curve behave almost linearly after 10 μm reaching an absorption of 40% at 300 μm.

The fluid chosen for this study is pure water, which is easy to handle, inexpensive and not toxic. Therefore, in Fig. 3, it is possible to compare the theoretical absorption and the one-term exponential approximation. The single "average" mean absorption coefficient chosen was derived from an experimental value. The use of a one-term approximation allows the inversion of the function, leading to a simple algebraic solution to the problem. The difference between the two curves increases with decreasing thickness, around 80% close to 0 μm, 20% at 50 μm, and lower than 8% at 100 μm. This difference is a monotone function, which can be quantified and corrected for after the data processing and the solution.

Inverting Equation (21) to find the actual integral average linear absorption coefficient of $\xi_{\lambda_1-\lambda_2}$ is not possible, hence as a first approximation, the choice of the use of a one-term linear absorption coefficient ξ_{100}, evaluated at liquid film thickness of 100 μm and a temperature of 30 °C in the exponential to determine the feasibility of the TBS technique. By inverting Equation (22) and using the result from Equation (19), it is possible to determine the thickness of the film L_F:

$$L_F = -\frac{1}{\xi_{100}} ln\tau_F \tag{23}$$

Note that the solution scheme can be implemented in two steps, using the film attenuation directly as unknown instead of its thickness and then solving independently the attenuation-thickness function and its inverse with more terms allowing the desired precision. It is to be mentioned that it is not possible to neglect at priory the linear absorption coefficient dependence on the fluid temperature. Nevertheless, with the given apparatus, we did not find any relevant difference in the measurement made with films at 15 °C and film at 45 °C on equivalent linear absorption coefficient. Its influence was lower than one order of magnitude than the signal noise and transmittance for the limited temperature range investigated.

3. Theoretical uncertainty analysis

Once defined the fluid with its corresponding physical properties, it is possible to apply the uncertainty propagation analysis to the theoretical model to find the relative error trend of the calculated thickness and the absolute uncertainty of the calculated temperature. The uncertainty of the measured thickness and temperature by the TBS technique can be expressed by Equation (23) and Equation (24), respectively.

$$u_{L_F}^2 = \left(\frac{\partial L_F}{\partial T_{S1}}\right)^2 u_{T_{S1}}^2 + \left(\frac{\partial L_F}{\partial T_{S2}}\right)^2 u_{T_{S2}}^2 + \left(\frac{\partial L_F}{\partial \xi_{100}}\right)^2 u_{\xi_{100}}^2 + \left(\frac{\partial L_F}{\partial T_{BG1}}\right)^2 u_{T_{BG1}}^2 + \left(\frac{\partial L_F}{\partial T_{BG2}}\right)^2 u_{T_{BG2}}^2 + \\ + \left(\frac{\partial L_F}{\partial \tau_w}\right)^2 u_{\tau_w}^2 + \left(\frac{\partial L_F}{\partial \varepsilon_{BG1}}\right)^2 u_{\varepsilon_{BG1}}^2 + \left(\frac{\partial L_F}{\partial \varepsilon_{BG2}}\right)^2 u_{\varepsilon_{BG2}}^2 \tag{24}$$

$$u_{T_F}^2 = \left(\frac{\partial T_F}{\partial S_1}\right)^2 u_{T_{S1}}^2 + \left(\frac{\partial T_F}{\partial S_2}\right)^2 u_{T_{S2}}^2 + \left(\frac{\partial T_F}{\partial \xi_{100}}\right)^2 u_{\xi_{100}}^2 + \left(\frac{\partial T_F}{\partial T_{BG1}}\right)^2 u_{T_{BG1}}^2 + \left(\frac{\partial T_F}{\partial T_{BG2}}\right)^2 u_{T_{BG2}}^2 + \\ + \left(\frac{\partial T_F}{\partial \tau_w}\right)^2 u_{\tau_w}^2 + \left(\frac{\partial T_F}{\partial \varepsilon_{BG1}}\right)^2 u_{\varepsilon_{BG1}}^2 + \left(\frac{\partial T_F}{\partial \varepsilon_{BG2}}\right)^2 u_{\varepsilon_{BG2}}^2 \tag{25}$$

For simplicity, it can be assumed that the setpoints which define T_{BG1} and T_{BG2} are accurate enough to neglect their uncertainty, as well as negligible are the uncertainties of the emissivity ε_{BG1}, and ε_{BG2} that can be estimated directly by a good infrared camera calibration. Then,

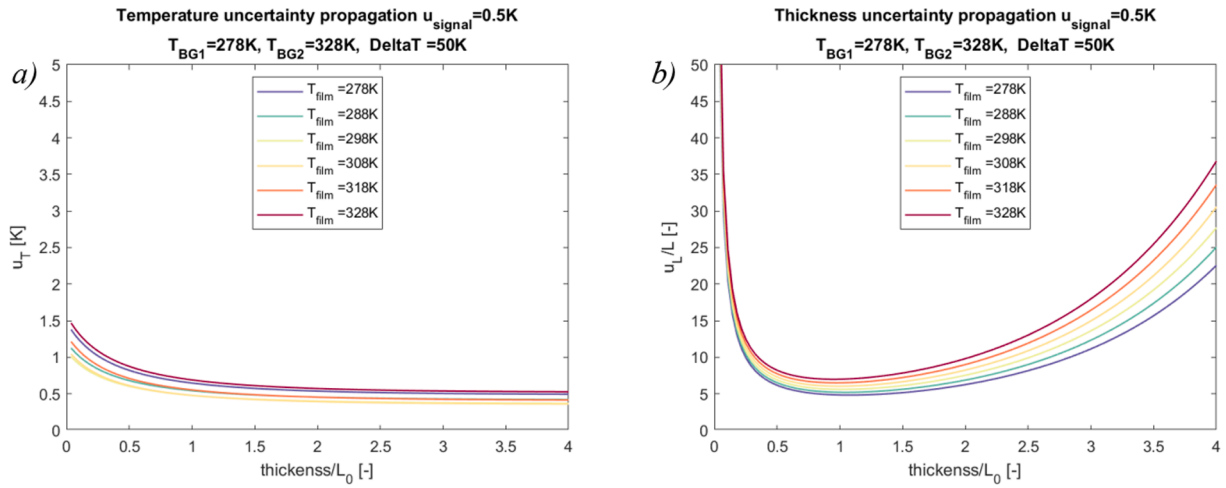

Fig. 4. Uncertainties propagation analysis with a temperature background difference of 50 K. a) Shows the temperature absolute uncertainty. b) Shows the thickness relative uncertainty.

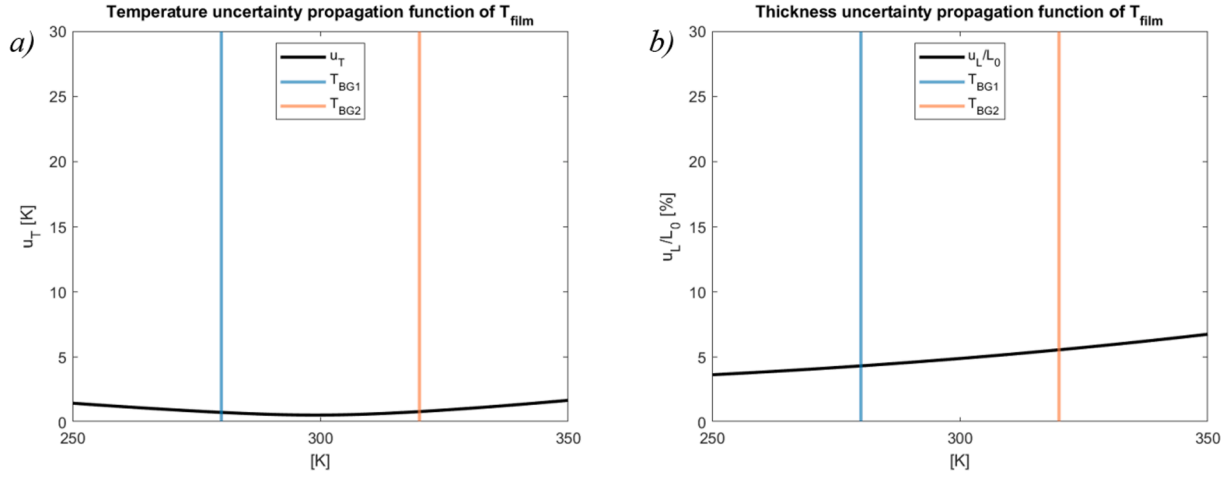

Fig. 5. Uncertainty propagation function of the film temperature. The two vertical lines represent the two background temperatures.

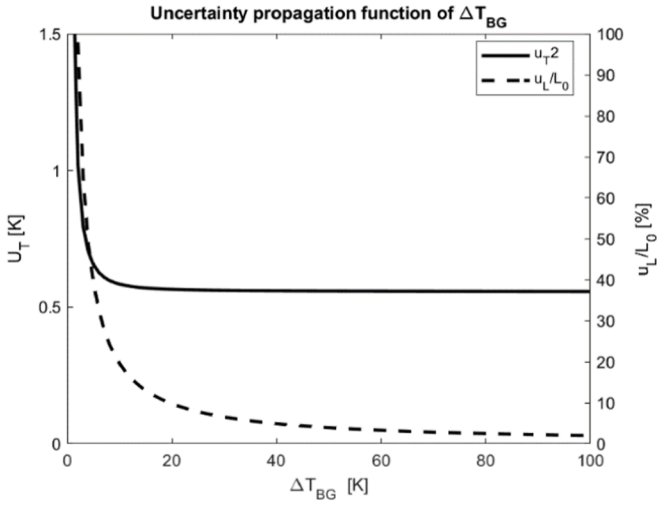

Fig. 6. Uncertainty propagation function of the backgrounds' temperature difference.

assuming both the uncertainty of the τ_W and ξ of 5% and applying an uncertainty of 0.5 K on the signals (expressed as apparent temperatures T_{S1}, T_{S2}) received and propagating it, both for the thickness and the temperature of the film, we obtain:

$$u_{L_F}^2 = \left(\frac{\partial L_F}{\partial T_{S1}}\right)^2 u_{T_{S1}}^2 + \left(\frac{\partial L_F}{\partial T_{S2}}\right)^2 u_{T_{S2}}^2 + \left(\frac{\partial L_F}{\partial \xi_{100}}\right)^2 u_{\xi_{100}}^2 + \left(\frac{\partial L_F}{\partial \tau_w}\right)^2 u_{\tau_w}^2 \quad (26)$$

$$u_{T_F}^2 = \left(\frac{\partial T_F}{\partial T_{S1}}\right)^2 u_{T_{S1}}^2 + \left(\frac{\partial T_F}{\partial T_{S2}}\right)^2 u_{T_{S2}}^2 + \left(\frac{\partial T_F}{\partial \xi_{100}}\right)^2 u_{\xi_{100}}^2 + \left(\frac{\partial T_F}{\partial \tau_w}\right)^2 u_{\tau_w}^2 \quad (27)$$

A parametrical analysis of the uncertainties is made by changing the background temperature difference and the fluid temperature. The analysis expressed the thickness normalized by the characteristic absorption length of the fluid $L_0 = -\frac{1}{\xi_{100}} = 55.56\,\mu m$, the inverse of the water average absorption coefficient at 100 μm, ξ_{100}. The analysis is shown in the following graphs highlighting the dependence on thickness, fluid temperature, and backgrounds temperature difference.

Fig. 4 shows the TBS technique uncertainties as a function of the thickness, with the reference temperature difference of 50 K between the two backgrounds ($T_{BG1} = 278$ K, $T_{BG2} = 328$ K) and by varying the film temperature in steps of 10 K between the two backgrounds. The results

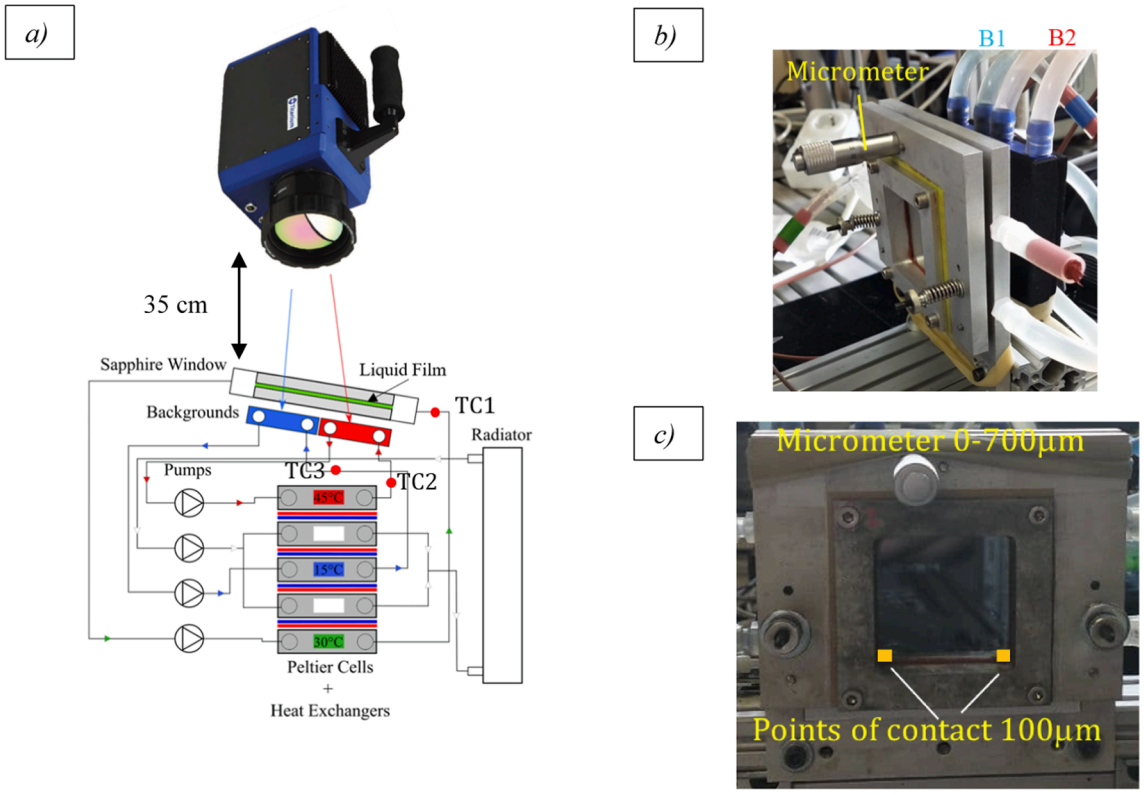

Fig. 7. A) TBS technique set-up scheme of the film widow, thermal control system and mwir camera, and b), c) the detail of the film window.

are shown in terms of *a)* temperature estimation absolute uncertainty and *b)* thickness estimation relative uncertainty. The colour of each line expresses the selected temperature of the film, from dark red (highest) to dark blue (lowest), but it will also be shown in detail in the next graphs. Both results show the uncertainty increasing exponentially when the real thickness approaches zero. This logically occurs when the layer of liquid is too thin, and its attenuation becomes negligible. When the film thickness increases, the temperature uncertainty decreases, reaching a horizontal asymptote dependent on the film's temperature, while the relative thickness uncertainty increases again. This occurs because when the thickness increases, the film begins to behave more like a fully opaque body; its temperature is measured directly with the uncertainty of the camera, but the difference between the two signals decreases to zero when the IR radiations coming from the backgrounds are no more discernible, so the relative errors dominate, and the film thickness is not measurable.

Analysing the film temperature effects on the uncertainty propagation, in Fig. 5, when the T_{film} is equal to the average of the two background temperatures, its uncertainty shows a minimum and increases when moving aside from this optimum. Focusing on the thickness uncertainties, it is possible to highlight that the uncertainty curve is monotonically increasing with no dependence on the two background temperatures.

Fixed the thickness to the previously defined characteristic absorption length L_0 and the film temperature T_{film} to 300 K, a higher background temperature difference decreases both the temperature uncertainty and the thickness relative uncertainty (see Fig. 6). The temperature uncertainty tends to be a horizontal asymptote function of the fluid temperature. The relative uncertainty of the fluid thickness tends asymptotically to zero. This uncertainty analysis concludes that the highest background temperature difference is optimal for the TBS technique. The maximum background difference constraint is not on an analytical level but on a thermophysical level: The maximum background temperature difference should be limited by the wish of not becoming intrusive so that a very hot background may heat up the film object of the investigation. The choice of these important parameters has to be carefully made in order to have a high "contrast" between the two signals but limiting the thermophysical effect on the film itself.

4. Experiment set-up

A validation set-up is designed and built in order to validate the TBS technique. The aim was to have a device having variable known film thickness and temperature to compare the results obtained by the TBS with the known values. Ideally, the experimental bench could be divided into four main parts: i) the liquid film window, ii) the backgrounds behind the film, iii) the temperature control system and the data logger, iv) and the infrared camera. Fig. 7 shows the scheme of the set-up, excluding the data logger:

- The mid-wave infrared camera (FLIR Titanium 520 M, 320 × 256 pixels, wavelength window 3.6 µm–5.1 µm), the film window, and the backgrounds are in-line (a slight tilt avoids the Narcissus effect).
- The film windows. The water film is contained in between two sapphire windows of 40 mm by 40 mm in an aluminium frame and hinged at their bottom corners spaced by 100 µm. The upper aluminium frame enables the variation of the top spacing, leading to the upper film variation between 0 and 500 µm.
- The two backgrounds, positioned 2 cm away from the sapphire windows, consist of a pair of commercial aluminum water-cooling blocks coated with high-emissivity black paint. They are insulated with 5 mm thick insulating foam on all surfaces that do not radiate to limit heat dissipation and transfer between the two bodies. The two radiating black bodies are installed on a sliding rail with two stops, which enables fast switching between them while maintaining the exact alignment.
- The temperature control is achieved by three thermostats controlling four Peltier's cells: one for the film liquid circuit, two in parallel for

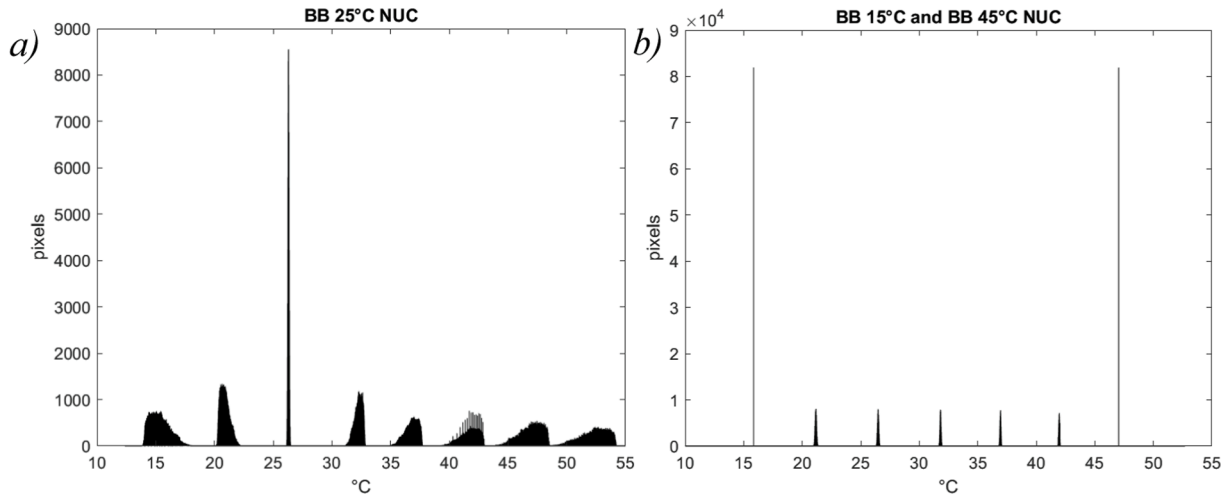

Fig. 8. Histogram of the temperature dispersion using a) one-point NUC; b) 2-point NUC.

the first background (cold) circuit and one for the second background (hot) circuit. The heat is exchanged between each circuit and a typical PC radiator to optimize the performance of the heat exchanger and for the best temperature control of the cold background. Four pumps (Syscooling SC-300 T, 300L/H) are used to circulate the water of each circuit and stabilize the temperature. The temperature of each circuit was maintained at the set temperature with a variation of no more than 0.3 °C. The circuits are color-coded for easier understanding. Red represents the hot background (B2) circuit, blue for the cold background (B1) circuit, green for the film circuit, and white for the hydraulic circuit of the dispelled heat.

The thin cavity of the two sapphire plates containing the film has a wedge shape resulting in a geometry similar to the study of Li et al. [22]. Three t-type thermocouples connected to a cRIO NI-9074 and NI-9214 module are installed at each background's water inlet and film window inlet. The temperature measurements are used as references to calibrate the thermal images in the data post-processing.

4.1. Infrared camera calibration

The set-up of the thermal camera and its operation is one of the most crucial aspects of the TBS technique. It may require a specific adaptation when a different device is used. A specific procedure was adopted to get reliable results from the thermal camera images by reducing temperature shifts during the experiment and minimizing the image noise and error. After the turn-on of the MWIR camera, a waiting period of two hours is allowed for the thermalization of the whole camera, which is equipped with a cryogenic Stirling cycle to cool down the sensor. Then a preliminary 1-point sensor non-uniformity correction (NUC) is performed before starting the measurements. NUC is a usual procedure for image acquisition which homogenizes the signal detected in the FOV or the gain for each pixel, both of which can vary differently with the integration time and the detector temperature and are subject to time drift. It corrects the offset thanks to a high emissivity black body at ambient temperature (in the following examples at 26 °C) that is positioned in front of the camera, with a tilting angle of 15° to avoid the cooled sensor auto reflection, also known as Narcissus effect. A second black body is positioned at 45° angle to reduce further the secondary reflections from the environment outside the field of view. After the first 1-point NUC, the following more accurate 2-point NUC is performed in the post-processing with two black body IR images taken at the temperature range extremes; it is used to improve the accuracy within the temperature range of interest. It exploits the same two backgrounds used by the TBS technique, one cold and the other hot, considered as two homogeneous surfaces, visualized at the whole field of view by the IR camera and used as two known fixed points to rescale the measurements. In Fig. 8, the histograms obtained with the 1-point NUC and the 2-point NUC show how the temperature dispersion over the images of a different black body at a constant homogeneous temperature is improved by applying this procedure.

In the graph on the left, a) the narrow peak at 26 °C shows the measured temperature of the calibration black block, and its dispersion shows the random error of the camera. The dispersion increases when the temperature moves away from the calibration at 26 °C; when the block at 55 °C is measured, 30 °C more than the calibration temperature, up to 4 °C of dispersion were reached, appearing in the images as a vignetting effect, with a colder border around the flatter central part of the image; in case of a colder block, a warmer vignetting appears. Graph b) on the right side shows the results after the 2-point NUC. It shows a dispersion lower than 0.3 °C with every homogeneous temperature. A possible systematic error can be corrected by measuring the fluid temperatures with other sensors.

The emissivity of the backgrounds and transmittance of the sapphire windows are found experimentally. The absorption coefficient for $L_F =$ 100 μm, ξ_{100}, was identified by selecting the two data of the temperature signals T_{S1} and T_{S2} with the top spacing at 100 μm to have the film shape as planar as possible and then choosing the region close to the bottom hinges. The ROI used was the same as identified in Fig. 7 c). By processing the data and solving the system of Equation (6), Equation (7) and Equation (22), the experimental absorption coefficient is found.

Fig. 9 shows how the TBS is applied to the series of image couples obtained. Two slightly convex windows contain the film, thus forming a concave wedge film with a maximum concavity of 40 μm. Two thermal images of the same film are obtained by switching the two backgrounds. Each image is the average of 10 frames taken at 10 Hz. Firstly, starting from the raw images of the thermal camera, a crop of the data to the ROI is made. Then a denoise of the data is done by using low-pass filtering on the temperature-reducing spikes and dead pixels, and then a temperature shift of the data is applied to match the fluid temperature data of the data logger thermocouples. Finally, by solving the equations Equation (6) and Equation (7), we calculate T_{film} and τ_{film}, and from equation

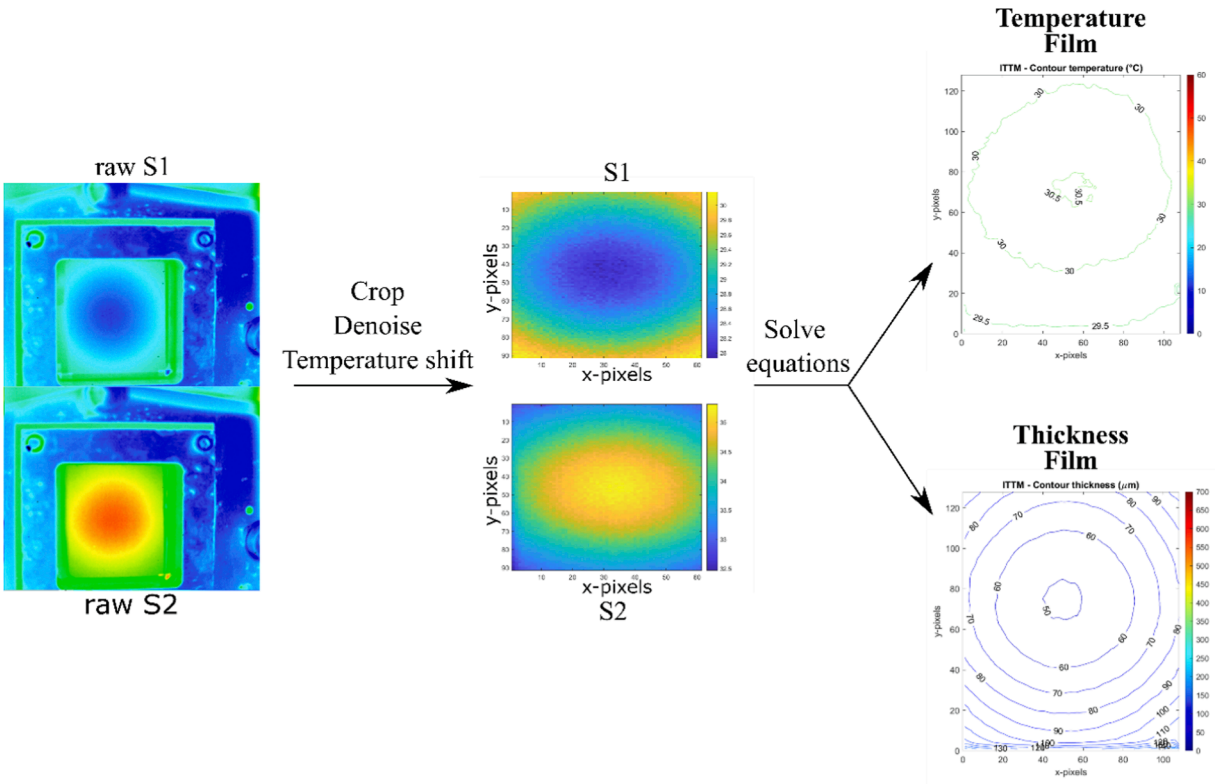

Fig. 9. TBS technique scheme method. The image is taken with a slightly concave film.

Equation (22), we can estimate the L_F. The experiments were carried out by fixing the temperature of the background at 15 °C and 45 °C respectively, by varying the film temperature from 15 °C to 50 °C with a 5 °C step and the distance at the top film edge from 0 μm to 500 μm with 15 μm steps from 0 μm to 320 μm and 50 μm and 60 μm steps afterwards.

5. Result

The film thickness and film temperature results obtained from the TBS technique are presented both as singular results and as global, the first showing the limit of the technique while the latter showing the reliability of the technique with an uncertainty analysis. Moreover, the technique has been proven against an optical technique.

5.1. Relevant results

As it was mentioned before, the film is contained in between the two sapphire plates in a wedge shape. Depending on the micrometre distance, we can select the shape of the wedge film. Moreover, the film presents a concavity at the centre of the two sapphire plates being not perfectly planar, hence causing a difference between the edge of the film and the centre of 40 μm. The following graphs show the result with T_F at 30 °C and with the top film thickness of 0 μm, 100 μm, 180 μm, and 350 μm respectively. Two graphs represent the infrared temperature and thickness measurements (ITTM) for the temperature and the thickness: a contour plot and a surface plot.

In Fig. 10, the top thickness of the film window is set to a minimum, with the two sapphire plates having a point of contact at around 100 y-pixels due to their slight convexity. This makes the thickness at the top not 0 μm but around 10 μm. At the minim of the concavity, the error increases for both the temperature measurements and the thickness leading to unreliable results. In particular, this behaviour is visible on the temperature graphs, where the decrease of thickness generates some results in the complex numerical domain and sharp peaks going towards unrealistic temperatures, around ± 400 °C. Contrary to this single result, the absolute error in thickness when it approaches zero seems to be low and is still able to catch the trend of the film without running into unrealistic measurements. The temperature error increases exponentially when the thickness is lower than 5 μm making the measurement completely unreliable. When the thickness is more than 10 μm, the temperature becomes almost constant on the entire film, with a difference across the film being around 0.5 °C.

Fig. 11 shows the results with the top distance of the wedge film set at 100 μm, equal to the bottom thickness at the hinge, hence in this case, the film variation is only dependent on the two sapphire plates containing the liquid the 40 μm central concavity formed by the two sapphire plates convexity. The temperature and the thickness results present the ideal case, where the error is minimal, and the TBS technique is highly sensitive to the thickness variation, while the measured temperature variation along the whole film is negligible. The effect of the radiation absorbed by the film has been estimated to be lower than 0.01 °C in the worst-case scenario. Moreover, the thermal inertia of the system containing the film is some orders of magnitude higher than the film. Thus once in a steady-state, it contributes to the temperature steadiness around the set point. Hence, the accuracy of the measured temperature with this technique depends mainly on the difference in detected temperature of the two signals, T_{S1} and T_{S2}.

Fig. 12 shows the results, with the top film thickness 170 μm. As before, the thickness range is still optimal, resulting in an extremely low variation in temperature along the whole film and very stable thickness measurement. However, it is to be noted that when increasing the thickness to more than 150 μm, the measured thickness starts to show some ripples.

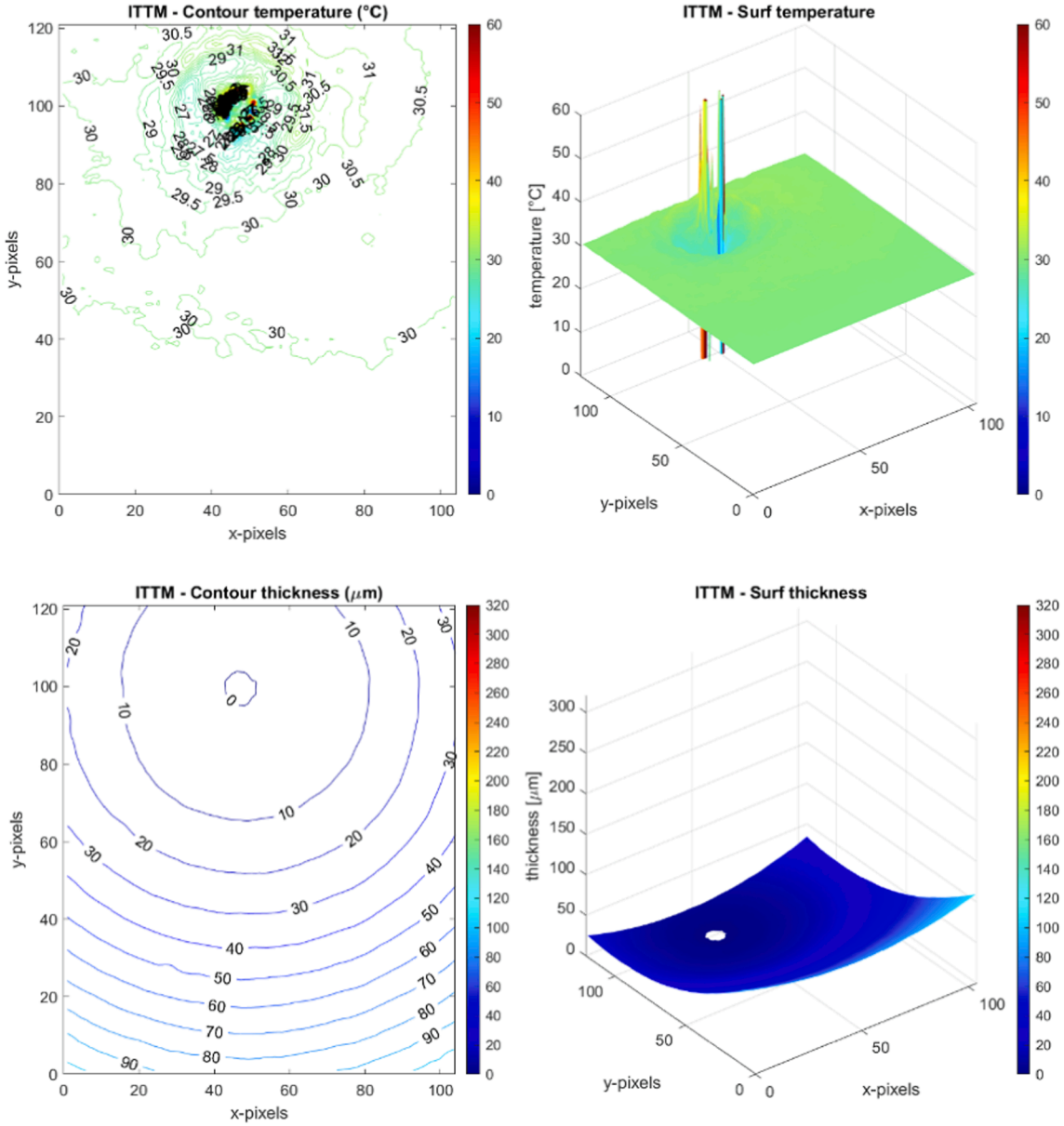

Fig. 10. Temperature and thickness results, top wedge 0 μm, $T_{film} = 30$ °C.

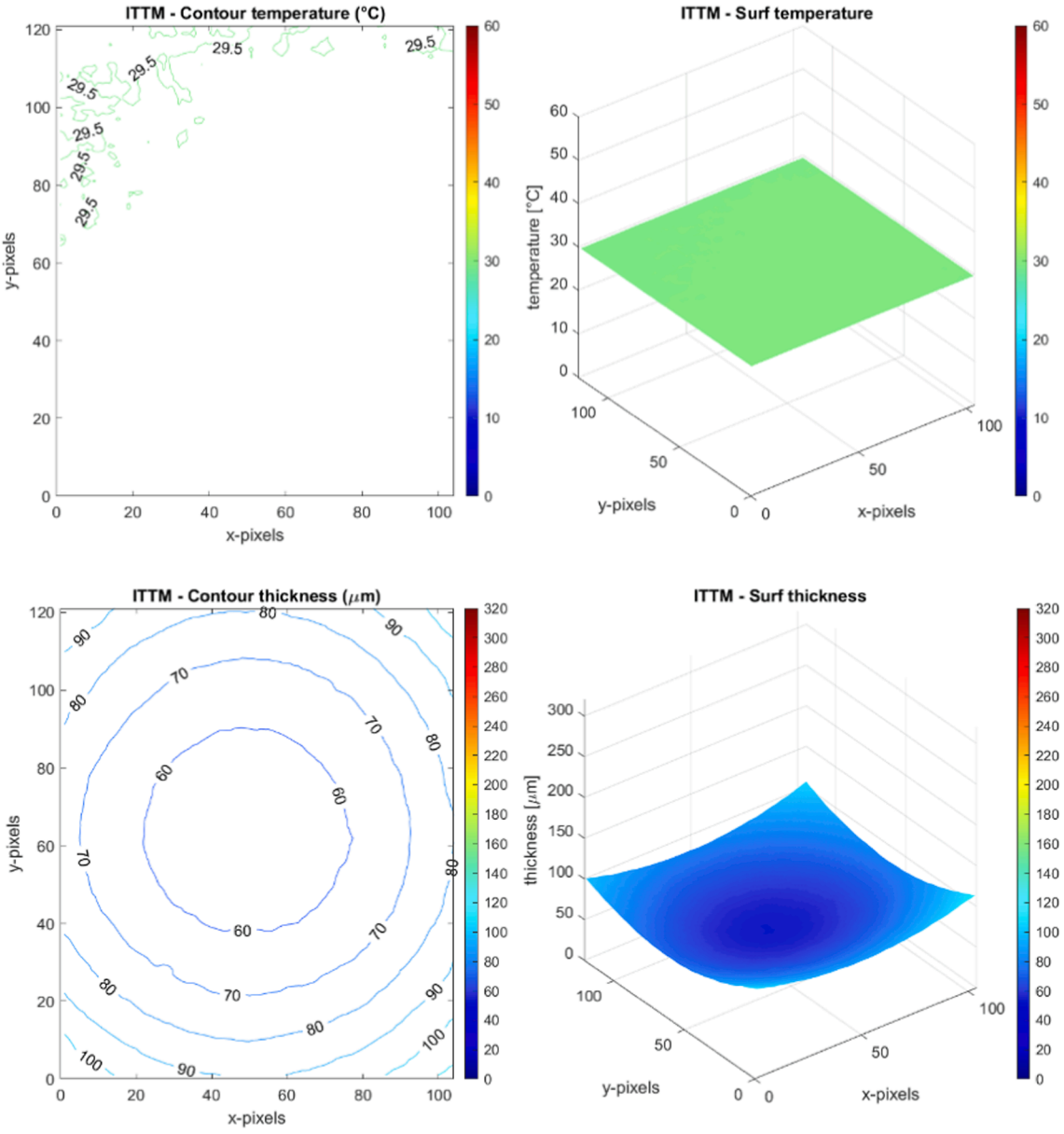

Fig. 11. Temperature and thickness results, top wedge 100 μm, $T_{film} = 30$ °C.

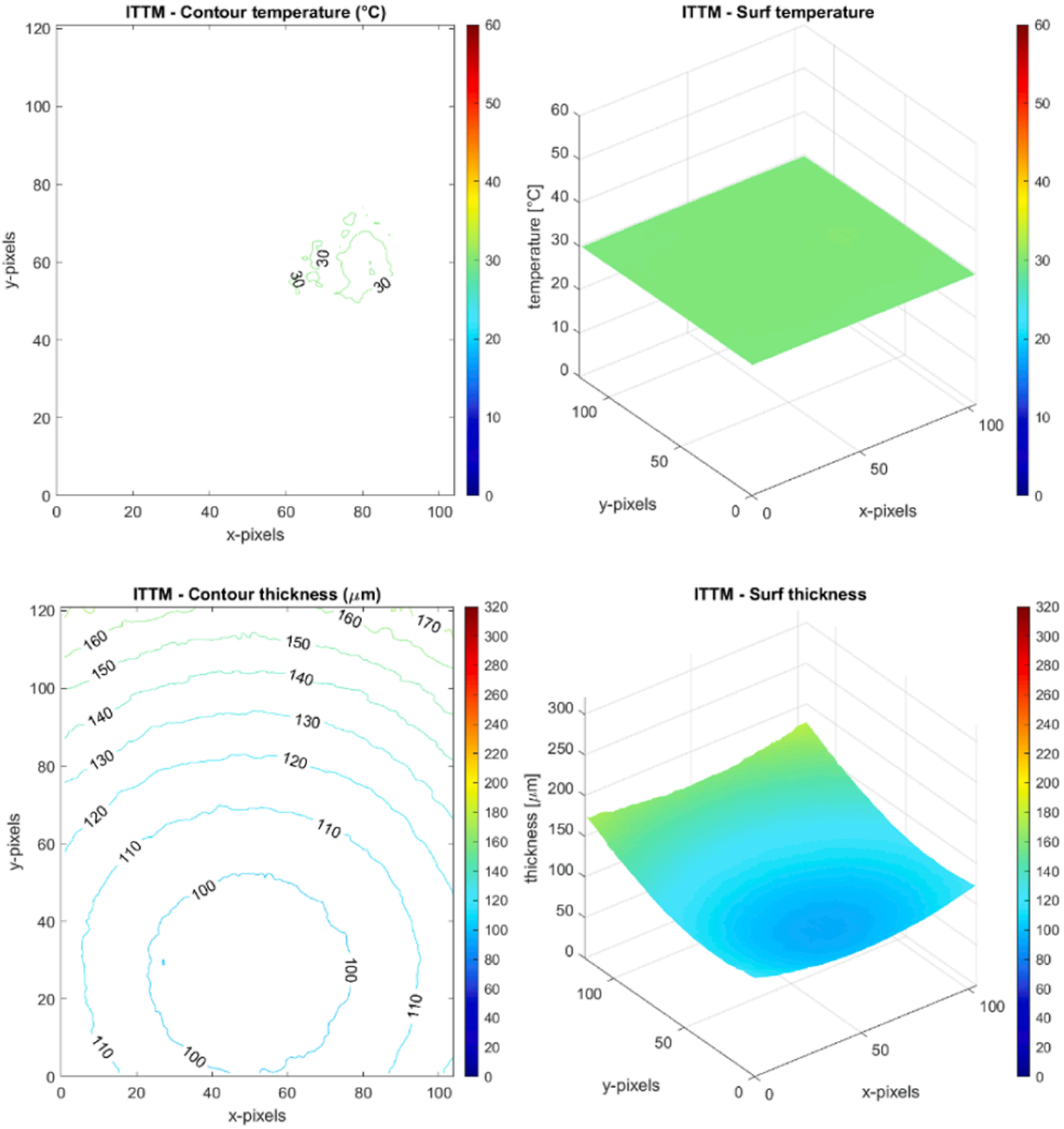

Fig. 12. Temperature and thickness results, top wedge 170 μm, T_{film} = 30 °C.

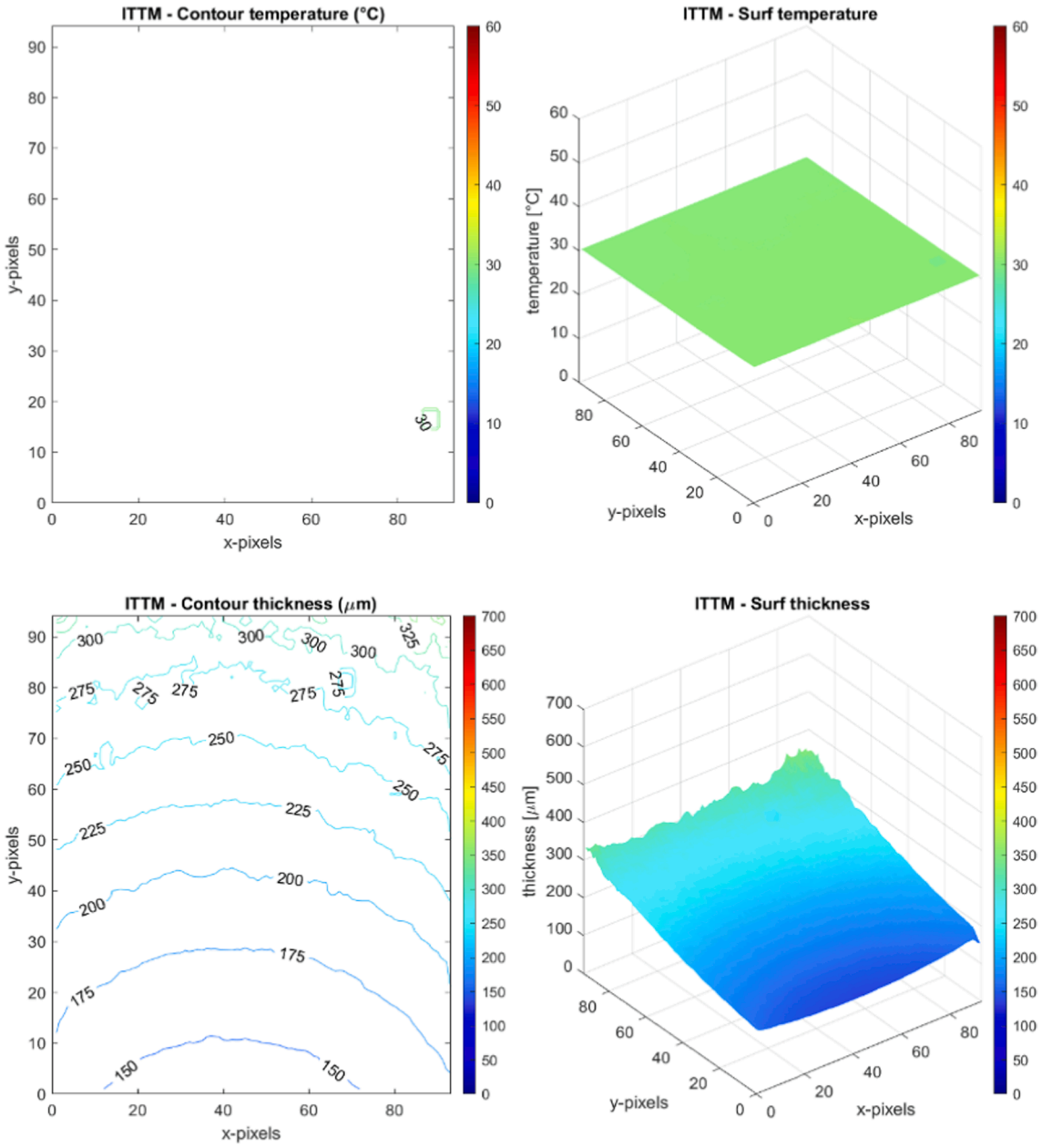

Fig. 13. Temperature and thickness results, top wedge 350 μm, T_{film} = 30 °C.

Fig. 13 shows the results when the upper distance of the wedge-shaped film is 350 μm. In these graphs, the high thickness results in an exceptionally low-temperature variation along the film because the film emissivity increases while its transmissivity is highly reduced, becoming more similar to an opaque body. The ripples caused by the noise generated by the TBS technique increase in the thickness graphs. Although the film trend is still recognisable, the measurement uncertainty is increasing, making the thickness estimation no more quantitatively reliable.

To evaluate the accuracy of the TBS measuring technique, not only was the thickness imposed by the two sapphire window shapes and micrometer action but the results were also proven against an optical technique in the visible spectrum working on the same principle of light attenuation by using an opaque fluid (water with black ink). Fig. 14 compares the thickness measured at each corresponding pixel by the two techniques for the 100 μm top thickness test. The results present a very good agreement between the two measurements.

5.2. Statistical results

To have a global analysis for all the tests performed and focus on the technique's random, non-systematic error, all the measurements in T_{film} and L_{film} were rearranged, binned by the 3x3 pixels mean thickness value measured, and then their average and dispersion were plotted. Then, this experimentally estimated random uncertainty is compared to the previous theoretical uncertainty analysis.

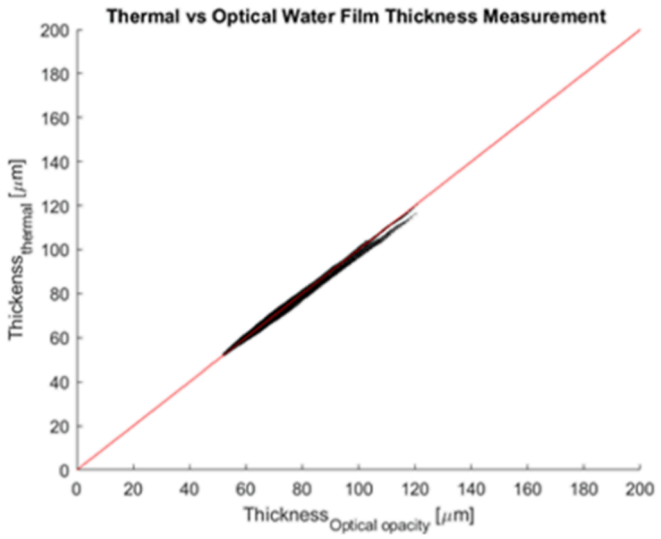

Fig. 14. Thickness thermal results against optical results.

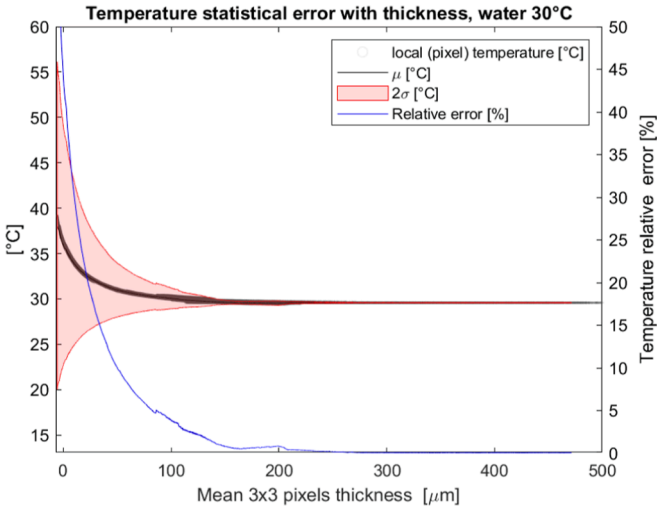

Fig. 15. Temperature error.

Fig. 15 focuses on all the measurements made by the TBS technique with the fluid temperature of 30 °C. The thickness on the x-axis is defined as the mean thickness across a 3x3 pixels matrix. The absolute error increases when the thickness tends to zero leading to a relative error that tends to infinite. The curve trend is equivalent to the theoretical uncertainty propagation, showing a dispersion higher than the theoretical one when the thickness is lower than 100 μm, decreasing towards uncertainty lower than 0.05 °C when the thickness is higher than 275 μm.

Fig. 16 shows the comprehensive experimental thickness uncertainty. Similarly to the previous theoretical analysis, the relative error curve shape is similar, confirming the previous result. On the contrary, from the experimental errors, the optimum range for the TBS technique is extended between 30 μm and 350 μm, with a relative error being lower than 5%.

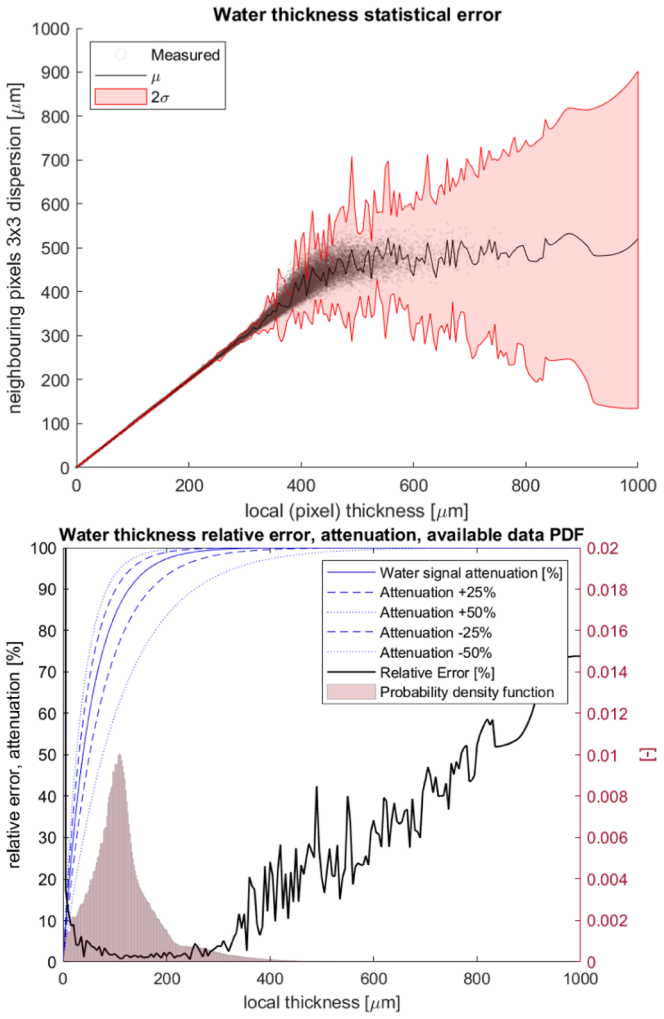

Fig. 16. A) Thickness absolute error, b) thickness relative error, and signal attenuation.

6. Possible applications and improvements

The proposed TBS technique can be further exploited by improving and changing the way the two signals are generated or collected, with the main aim of collecting the two signals simultaneously. Possible examples of experimental configurations are:

- Infrared stereoscopy, by the use of two cameras, targeting at the same film region but then different background surfaces.
- Stereoscopy with one single camera, exploiting two optical paths tanks to appropriate tilted infrared mirrors behind the investigated film. This configuration is well suited for cylindrical symmetric films inside a transparent tube.
- High-speed MEMS micro mirrors, alternatively switching from different backgrounds signals.
- Matrix of alternate points or stripes of high reflection and high emissivity of the same surface. At the cost of a lower spatial resolution, it would allow simultaneous acquisition and high temporal resolution with a single camera. It may use the opaque surface onto which the film is deposed as background after proper preparation.

- Use of high-speed infrared LEDs to illuminate a partially reflective background changing at high frequency its radiation characteristics.
- Use of two cameras, or filters, with different waveband responses to which the film shows significantly different extinction coefficients.

The TBS technique's next step should be focused on the application to dynamic problems. It is in the program to apply it on a bi-phase flow inside channels to investigate the thermofluidic dynamic of the liquid film around moving bubbles in small circular channels. Moreover, with slight adaptations, the principles and the algorithm of the TBS technique have high potential and can also be applied for other film problems like the measure of concentration inside mixtures of liquids and solutions.

7. Conclusion

The novel technique presented, named Twin Background Subtraction, was successfully studied and developed to measure the temperature and the thickness of a semi-transparent thin film. The technique exploits the infrared images from a commercial infrared camera, so it can have a wide field of view compared to the majority of the techniques present in literature, which are local. The applicability of the Twin Background Subtraction technique for a wide range of film thickness has been confirmed both theoretically and experimentally. When using water as liquid film, the results show that the thickness measurements can have an uncertainty lower than 5% between 50 and 350 μm; hence the technique range of applicability is wider than what was previously supposed by 75%. Qualitatively the results are also valid for microfilm as thin as 10 μm. For thinner films, the error is too high and gives unrealistic measurements. The temperature measurements show a decreasing error with the thickness increase, but as for the thickness measurements, the technique uncertainty spikes toward infinite when the film thickness tends to zero. The error also depends on the temperature of the film and the two backgrounds temperature difference; the optimum measurement range is between the two background temperatures. The increase in the backgrounds' temperature difference will increase the accuracy of the final measurements because it will increase the sensitivity of the TBS technique. The favourable difference in the experimental uncertainty estimation is probably due to the instrument's real accuracy being better than the overestimating values assumed in the theoretical analysis, allowing us to consider possible further improvements of the technique with accurate set-up and calibration. Finally, the TBS technique has proven to be an interesting tool for the study of different thermofluidic problems, like but not limited to condensation, confined flows in channels, and flow boiling.

CRediT authorship contribution statement

R. Clavenna: Conceptualization, Investigation, Software, Validation, Methodology, Formal analysis, Data curation, Writing – review & editing. **L. Araneo:** Conceptualization, Validation, Formal analysis, Data curation, Supervision, Writing – review & editing.

Declaration of Competing Interest

The authors declare that they have no known competing financial interests or personal relationships that could have appeared to influence the work reported in this paper.

Data availability

Data will be made available on request.

Acknowledgements

The present work is carried forward in the framework of the project "Two-Phase Passive Thermal Devices For Deployable Space Systems (TOPDESS)", financed through the Microgravity Application Program (MAP N. 4000128640) by the European Space Agency.

References

[1] C.B. Tibiriçá, F.J. Nascimento, G. Ribatski, Film thickness measurement techniques applied to micro-scale two-phase flow systems, Exp. Therm. Fluid Sci. 34 (2010) 463–473.
[2] G. Mignot, et al., Measurement of liquid films thickness in a condensing and re-evaporating environment using attenuation of near infrared light, Nucl. Eng. Des. 336 (2018) 64–73.
[3] J. Dupont, G. Mignot, D. Paladino, H.M. Prasser, Mid wave infrared thermography of water films in condensing and evaporating environments, Nucl. Eng. Des. 336 (2018) 80–89.
[4] T. Morokuma, T. Ohara, Y. Utaka, Combination of laser interferometric and laser extinction methods for precise thickness measurement of liquid film between coalescing twin air bubbles, Int. J. Heat Mass Transf. 127 (2018) 154–160.
[5] A. Schmidt, et al., Laser based measurement of water film thickness for the application in exhaust after-treatment processes, Int. J. Heat Fluid Flow 71(October 2017) (2018) 288–294.
[6] Y. Han, Shikazono,, Measurement of the liquid film thickness in micro tube slug flow, Int. J. Heat Fluid Flow 30 (5) (2009) 842–853, https://doi.org/10.1016/j.ijheatfluidflow.2009.02.019.
[7] T. Xue, L. Yang, P. Ge, L. Qu, Error analysis and liquid film thickness measurement in gas-liquid annular flow, Optik (Stuttg) 126 (20) (2015) 2674–2678.
[8] A.V. Cherdantsev, J.S. An, A. Charogiannis, C.N. Markides, Simultaneous application of two laser-induced fluorescence approaches for film thickness measurements in annular gas-liquid flows, Int. J. Multiph. Flow 119 (2019) 237–258.
[9] A. Bonilla Riaño, I.H. Rodriguez, A.C. Bannwart, O.M.H. Rodriguez, Film thickness measurement in oil-water pipe flow using image processing technique, Exp. Therm. Fluid Sci. 68 (2015) 330–338.
[10] A. Donniacuo, R. Charnay, R. Mastrullo, A.W. Mauro, R. Revellin, Film thickness measurements for annular flow in minichannels: Description of the optical technique and experimental results, Exp. Therm. Fluid Sci. 69 (2015) 73–85.
[11] M. Wang, D. Zheng, Y. Xu, A new method for liquid film thickness measurement based on ultrasonic echo resonance technique in gas-liquid flow, Meas. J. Int. Meas. Confed. 146 (2019) 447–457.
[12] M. Yu, L. Shen, T. Mutasa, P. Dou, T. Wu, T. Reddyhoff, Exact analytical solution to ultrasonic interfacial reflection enabling optimal oil film thickness measurement, Tribol. Int. 151 (June) (2020).
[13] R. Wang, B.A. Lee, J.S. Lee, K.Y. Kim, S. Kim, Analytical estimation of liquid film thickness in two-phase annular flow using electrical resistance measurement, Appl. Math. Model. 36 (7) (2012) 2833–2840.
[14] R. Tiwari, M. Damsohn, H.M. Prasser, D. Wymann, C. Gossweiler, Multi-range sensors for the measurement of liquid film thickness distributions based on electrical conductance, Flow Meas. Instrum. 40 (2014) 124–132.
[15] C.J. Choi, H.K. Cho, Investigation on emergency core coolant bypass with local measurement of liquid film thickness using electrical conductance sensor fabricated on flexible printed circuit board, Int. J. Heat Mass Transf. 139 (2019) 130–143.
[16] W. Wu, S. Kong, X. Xu, J. Tao, C. Li, J. Wang, M. Su, H. Yang, Simultaneous measurement of liquid film thickness and temperature on metal surface, Spectrochim. Acta A 257 (2021), https://doi.org/10.1016/j.saa.2021.119804.
[17] M. Abela, M. Mameli, V. Nikolayev, S. Filippeschi, Experimental Analysis and transient numerical simulation of a large diameter pulsating heat pipe in microgravity conditions, Int. J. Heat Mass Transfer 2022, January 19. https://doi.org/10.1016/j.ijheatmasstransfer.2022.122532.
[18] M. Mameli, A. Catarsi, D. Mangini, L. Pietrasanta, N. Michè, M. Marengo, P.D. Marco, S. Filippeschi, Start-up in microgravity and local thermodynamic states of a hybrid loop thermosyphon/pulsating heat pipe, Appl. Therm. Eng., 2019, May 13, https://doi.org/10.1016/j.applthermaleng.2019.113771.
[19] The Ultimate Infrared Handbook for R&D Professionals, https://www.flir.com/discover/rd-science/the-ultimate-infrared-handbook-for-rnd-professionals/.
[20] Refractive index database. Optical constants for crystals. July 2019. url: https://refractiveindex.info/?shelf=3d&book=crystals&page=sapphire.
[21] The HITRAN Database,. November 2021, url: https://hitran.org/.
[22] T. Li, T. Lian, B. Huang, X. Yang, X. Liu, Y. Li, Liquid film thickness measurements on a plate based on brightness curve analysis with acute PLIF method, Int. J. Heat Mass Transf. 136 (2021), https://doi.org/10.1016/j.ijmultiphaseflow.2020.103549.